JOURNAL OF SOLID STATE CHEMISTRY 103, 322–333 (1993)

Structural Characterization and Polymorphism of R_2BaNiO_5 (R = Nd, Gd, Dy, Y, Ho, Er, Tm, Yb) Studied by Neutron Diffraction

E. GARCÍA-MATRES, J. L. MARTÍNEZ,* AND J. RODRÍGUEZ-CARVAJAL†

*Institut Laue–Langevin, B.P. 156X, F-38042, Grenoble Cedex-9, France, and *Instituto de Ciencia de Materiales de Madrid (C.S.I.C.), Fac. Ciencias (C-4), Universidad Autónoma de Madrid, E-28049 Madrid, Spain*

J. A. ALONSO

Instituto de Ciencia de Materiales de Madrid, C.S.I.C. Serrano 113, E-28006 Madrid, Spain

AND A. SALINAS-SÁNCHEZ AND R. SAEZ-PUCHE

Dep. Química Inorgánica, Fac. de Ciencias Químicas, Universidad Complutense E-28040 Madrid, Spain

Received June 2, 1992; in revised form September 4, 1992; accepted September 11, 1992

The family of compounds R_2BaNiO_5 (R = Nd, Dy, Y, Ho, Er, Tm, Yb) has been studied by neutron powder diffraction at room temperature. All of them present orthorhombic symmetry (space group *Immm*, $Z = 2$). The main feature of these materials is the existence of one-dimensional chains of vertex-sharing NiO_6 octahedra along the a-axis. The present research has revealed the effect of the size of the rare earth ions on the structural parameters, which plays a role nearly equivalent to a hydrostatic "chemical pressure" in the geometric distortion of the structure. The volume of the Ni and Ba polyhedra varies linearly vs the ionic radius of the rare earth. The overall agreement between the valence bond sums and formal charges is very poor. This fact indicates that the present structure is under very high internal stress and may be metastable. We speculate that there may exist a dimorphism in the other members of this family of oxides, similar to that already found for the Tm, Yb, and Lu compounds.

Introduction

After the discovery of high T_C superconductivity, many investigations were made looking for new high temperature superconductor oxides. For that reason earlier work with similar oxides was carefully reanalyzed. The initial work on the family of compounds with general formula Ln_2BaMO_5 (M = Co, Ni, Cu, Pd, Pt, Mn, Zn; Ln = Nd, Sm, Eu, Gd, Dy, Ho, Er, Tm, Yb, Lu, Y) was done in great detail by Müller-Buschbaum's group (*1–12*) and by Michel and Raveau (*13, 14*).

† Present address: Laboratoire Léon Brillouin (CEA-CNRS), Centre d'Etudes de Saclay, F-91191 Gif sur Yvette Cedex, France.

0022-4596/93 $5.00

These compounds are insulators and present new structural types and many interesting magnetic properties. They can be classified into four types of structures, depending on the different oxygen coordinations of the divalent M^{2+} cations (*1–16*). The possible coordinations are square planar (P) or tetrahedral (T) (coordination 4, i.e., C4P or C4T), square pyramidal (C5), and octahedral (C6).

The first structural type is represented by Nd_2BaMO_5 (M = Pt, Pd, Cu) with square planar coordination of the M metal (C4P). $La_{2-x}Ba_{1+x}CuO_{5-\delta}$ also belongs to this structure. It is worth noting that the planar coordination for M is only possible in the case of the larger rare earth atoms.

The second structural type is represented by Nd_2BaZnO_5, belonging to the space group *I4/mcm*. This system is characterized by the presence of ZnO_4 tetrahedral groups (C4T) (*15*).

The third structure, with square pyramids (C5), which is the most frequent coordination for M (*16, 17*), is represented by Sm_2BaCuO_5 (space group *Pnma*). Compounds with this structural type have been described for M = Cu, Ni, or Co and different rare earths. In the case of copper they were called "green phases" when they were found as a contamination during the synthesis of the well known $RBa_2Cu_3O_{7-x}$ superconductors. In the case of nickel, the compounds of the smaller rare earths (Tm, Yb, or Lu) also crystallize in this structure (*16*).

The fourth, and last, structural type is represented by Nd_2BaNiO_5 (space group *Immm*), in which the coordination of Ni^{2+} is an octahedron (C6) of oxygens. Only compounds with Ni or Co and the bigger rare earth atoms are known to present this structure.

In the case of nickel (*18–20*), the oxides of formula R_2BaNiO_5 with R = Lu, Yb, Tm, Er, Ho, Y, Dy, Gd, Nd present frequently an octahedral coordination of Ni^{2+}. Usually, for the smallest lanthanides such as Tm^{3+}, Yb^{3+}, or Lu^{3+}, the system is stable in the third structural type with Ni^{2+} in pyramidal coordination. However, Tm_2BaNiO_5 (*21*) and Yb_2BaNiO_5 are actually dimorphic and can be stabilized in two different structures with Ni ions in pyramidal or octahedral coordination, depending on the synthesis conditions. These compounds are probably a limit of stability for this structural type and certainly deserve a deeper study. From now on we concentrate on the fourth structural type.

In order to name the different compounds we propose to use the following nomenclature. Hereafter we shall use a short symbol to represent "rare earth (transition metal)-coordination of the transition metal." For example, Tm(Ni)-C6 means the compound Tm_2BaNiO_5 crystallizing in the phase with NiO_6 octahedra (fourth structural type). The second polymorph will be denoted as Tm (Ni)-C5, i.e., Tm_2BaNiO_5 with NiO_5 square pyramids (third structural type).

The most important structural feature of the R(Ni)-C6 family is the existence of isolated chains of NiO_6 flattened octahedra along the a-axis (see Fig. 1). The space group is *Immm* (Z = 2), which requires that all four Ni–O(1) bonds be in the equatorial plane, perpendicular to the [100]-axis, and of equal length. Direct oxygen bonds between chains are absent, so the chains are magnetically isolated, being linked through the R^{3+} and Ba^{2+} ions. The most spectacular features are observed for Y_2BaNiO_5, in which the chains are linked only by diamagnetic cations Ba^{2+} and Y^{3+}. Because of that, the magnetic interchain interactions are weak and Ni^{2+} behaves as a nearly pure one-dimensional antiferromagnetic system without 3D antiferromagnetic ordering above 1.5 K. This behavior implies many interesting magnetic properties, as can be observed in magnetic susceptibility and neutron diffraction measurements (*22–25*). In fact, the Y compound could be considered as a prototype of the one-dimensional Heisenberg antiferromagnet with S = 1. The introduction of paramagnetic rare earth

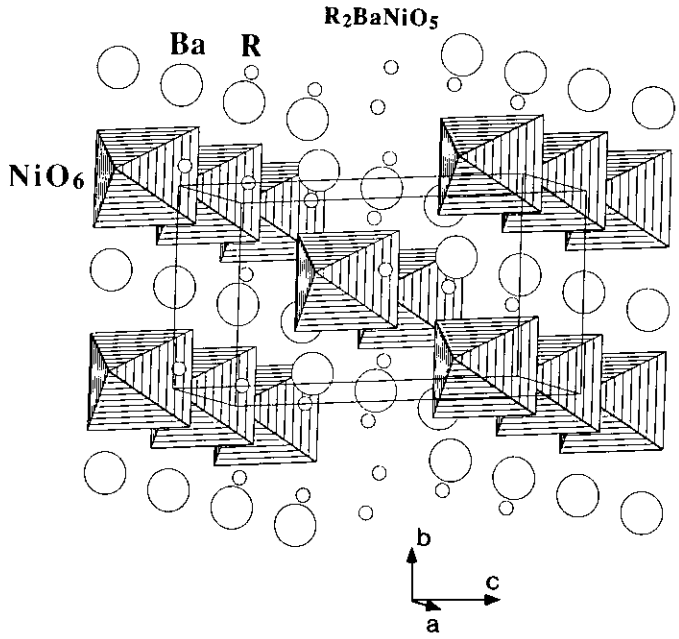

FIG. 1. View of the R_2BaNiO_5 structure (R(Ni)-C6 structural type) showing the NiO_6 octahedra chains.

ions modifies the magnetic behavior of R_2BaNiO_5 and simultaneous 3D antiferromagnetic ordering of the rare earth and Ni sublattices is observed at rather high temperatures (*22–25*). One of the aims of the present study is to accurately determine all the structural parameters of this peculiar materials, in order to get a deeper insight into the stability of this structure. This study is also necessary before the detailed analysis of the microscopic magnetic properties is attempted.

Experimental Details

Different R_2BaNiO_5 (R = Y, Nd, Dy, Ho, Tm, Er and Yb) samples of R(Ni)-C6 type were prepared as polycrystalline materials by solid state reaction from stoichiometric mixtures of analytical grade R_2O_3 (99.99%), NiO (99.999%), and $BaCO_3$ (A.R. grade). The samples were ground, pelletized and heated in air at 900°, 1000°, 1100°, and 1200° C for 12 hr. After each thermal treatment the reaction products were cooled rapidly, reground, and pelletized. For the Yb compound BaO_2 was used instead of barium carbonate. The sample was heated up to a maximum temperature of 1050°C. Further heatings led to the transformation to the Yb (Ni)-C5 polymorph. It is interesting to comment that the Lu compound, described until now as Lu(Ni)-C5, could also be identified in its Lu(Ni)-C6 form at 1100°C, but we were not able to prepare it as a single phase.

Neutron powder diffraction experiments were carried out in the High Flux Reactor at the Institut Laue–Langevin (Grenoble, France). The diffraction patterns were collected on the high resolution diffractometer D2B with λ = 1.594 Å working in the high flux mode. This diffractometer is equipped with a bank of 64 detectors separated 2.5° in 2θ, spanning an angular range of 160° (2θ). Each detector is equipped with Soller slits. Scanning the detector bank by 2.5°, in steps

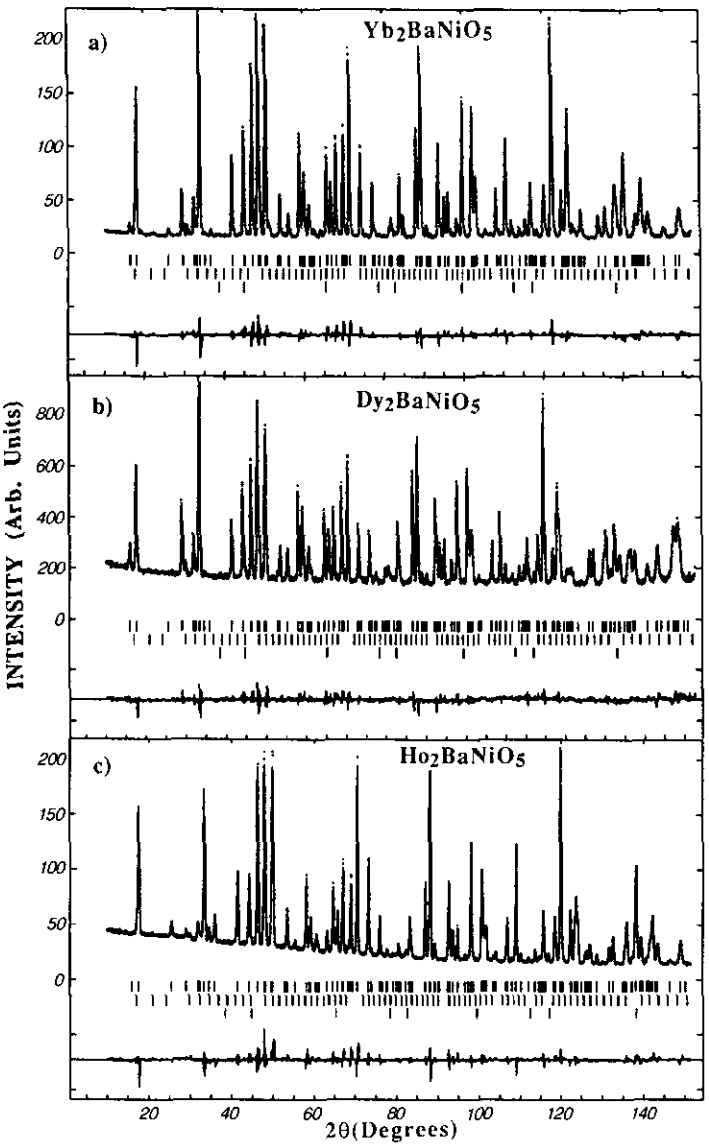

FIG. 2. Neutron powder diffraction pattern at RT for (a) Yb_2BaNiO_5, (b) Dy_2BaNiO_5, and (c) Ho_2BaNiO_5. The solid line is the calculated profile; vertical marks show the positions of allowed reflections for the main phase and the two impurities R_2O_3 and NiO. The difference curve is also plotted at the bottom part of each frame.

of 0.05° one gets a full diffraction pattern. This wide angular range (160°) corresponding to a Q range below 7.76 $Å^{-1}$ ($d_{min} \approx$ 0.81 Å) allows the accurate analysis of fine structural details.

All data were analyzed with the Rietveld method using the program FULLPROF (*26*). This program allows the simultaneous fitting up to eight phases, including magnetic structures. The background was a polynomial re-

TABLE I

STRUCTURAL PARAMETERS AND RELIABILITY FACTORS OF THE FITTING FOR R_2BaNiO_5 (R = Nd, Dy, Y, Ho, Er, Tm, Yb) FROM HIGH RESOLUTION POWDER DIFFRACTION DATA AT ROOM TEMPERATURE

		Nd	Dy	Y	Ho	Er	Tm	Yb
Lattice parameters:								
a		3.82795(6)	3.77414(5)	3.76222(4)	3.76370(4)	3.75439(8)	3.75124(4)	3.74482(4)
b		5.93211(9)	5.78000(8)	5.76271(8)	5.76101(8)	5.7446(2)	5.72140(8)	5.70668(8)
c		11.6618(2)	11.3641(1)	11.3337(1)	11.3357(1)	11.3018(3)	11.2456(1)	11.2040(1)
Volume (Å^3)		264.81	247.90	245.72	245.79	243.75	241.36	239.44
R (1/20z)	4j							
z		0.2027(1)	0.20321(7)	0.2022(1)	0.2028(1)	0.2029(2)	0.2033(1)	0.20323(7)
B(Å^2)		0.45(2)	0.34(2)	0.57(2)	0.41(2)	0.4(5)	0.54(3)	0.44(2)
Ba (1/21/20)	2c							
B(Å^2)		0.96(5)	1.26(7)	1.04(5)	1.02(5)	0.88(5)	1.06(5)	0.86(5)
Ni (000)	2a							
B(Å^2)		0.62(3)	0.50(3)	0.57(2)	0.65(3)	0.39(5)	0.68(3)	0.51(3)
O(1) (0yz)	8l							
y		0.2419(3)	0.2412(4)	0.2403(3)	0.2410(3)	0.2414(7)	0.2399(4)	0.2393(3)
z		0.1444(1)	0.1485(2)	0.1492(1)	0.1488(1)	0.1483(2)	0.1499(1)	0.1504(1)
B(Å^2)		0.82(2)	0.63(3)	0.73(2)	0.80(2)	0.56(4)	0.82(2)	0.70(3)
O(2) (1/200)	2b							
B(Å^2)		0.98(4)	0.87(5)	0.76(4)	0.74(3)	0.40(6)	0.76(4)	0.68(4)
Number of reflections		175	164	154	158	152	159	156
Reliability factor (%):								
R_{wp}		6.21	4.02	8.15	5.07	8.64	6.71	5.81
R_{exp}		2.26	2.86	4.41	2.64	4.12	4.56	2.33
χ^2		7.57	1.98	3.42	3.69	4.39	2.17	6.24
R_B		5.42	4.42	4.04	4.71	10.4	4.64	4.64

Note. Coherent scattering lengths (fm) are b_{Ni} = 10.3, b_O = 5.803, b_{Ba} = 5.25, b_{Nd} = 7.69, b_{Dy} = 16.9, b_{Ho} = 8.08, b_Y = 7.75, b_{Er} = 8.03, b_{Tm} = 7.05, and b_{Yb} = 12.40. Space Group $Immm$ (Z = 2). At variance with previous works, the origin has been taken at the Ni position.

finable function, and R_2O_3 (cubic, $Ia3$) and NiO (cubic, $Fm3m$) phases were included as impurities in all the profile refinements. The maximum weight fraction of impurity phases was in all cases smaller than 1%.

Absorption corrections for cylindrical samples were applied considering a packing factor for the powder of 0.5. This has only the effect of slightly modifying the atomic thermal parameters. In the case of Dy(Ni)-C6, the neutron diffraction pattern was obtained using a specially designed hollow sample holder, in order to diminish the high absorption coming from Dy.

Experimental Results

Neutron powder diffraction patterns were obtained at room temperature (RT) for R_2BaNiO_5 oxides with the following rare earths R = Yb, Tm, Er, Ho, Y, Dy and Nd. In the case of Er we used the data already published (*27*). Figure 2 shows the observed and calculated neutron diffraction patterns for some of these compounds. It is important to point out that Yb_2BaNiO_5 was until now described as Yb(Ni)-C5.

Table I gives the summary of refined parameters for this family of oxides: cell parameters, atomic positions, isotropic temperature factors, and reliability factors. The results are consistent with previous data when these exist (*1–12, 19–21, 25, 27*). The difference in the thermal factors for Er(Ni)-C6 with Ref. 27 comes from the application of the absorption correction in the present work. It is worth noting that with high-resolution neutron powder diffraction it is possible to obtain better accuracy in the location of oxygen atoms than in the case of X-ray diffraction (even from single crystals).

We also fit the data with anisotropic

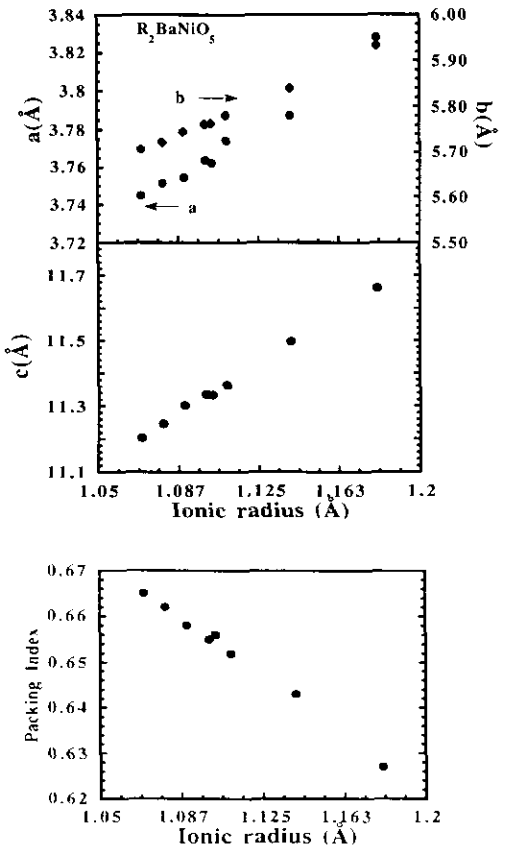

FIG. 3. Lattice parameters a, b, and c vs rare earth ionic radius. The packing index is also included in the lower frame (c). Data for Gd oxide in all the figures are from Ref. (*19*).

atomic thermal factors, to take into account the noncubic site symmetry present in this structure. The corresponding atomic displacements along the crystallographic axes do not indicate very strong anisotropic behavior, as is also reflected in the similar values of the R-factors for the isotropic and anisotropic refinements. The only significant trend we observed is that the displacements of Ni and O(2) along the b-axis are almost one order of magnitude larger than those along the two other crystallographic axes. This fact is consistent with the softer O(2)-Ba bond, directed along [010], which is reflected also in the high variation of its length with the different rare earths (see below). However the displacements are small, suggesting that the atoms are very well fixed in their special positions without presenting any sign of disorder. Because not much improvement is obtained by the use of anisotropic thermal factors, only the isotropic factors are presented in Table 1.

The upper frames of Fig. 3 illustrates the lattice parameters of the different R_2BaNiO_5 oxides vs the ionic radii of the rare earth atom. For the ionic radii we have used those quoted in Ref. (*28*); any other values given in the literature do not affect the discussion presented below. The relative variation of the three axes is different. b and c axes vary around $\pm 2\%$ over the average value, however the relative variation of the a-axis is only $\pm 1.1\%$. As expected from the ionic model, the unit cell volume increases as does the ionic radius. The maximum variation over the average volume value is $\pm 5\%$.

Another interesting point is the fact that the packing index of the structure also depends linearly on the size of the rare earth. The packing index is calculated as the ratio between the atomic and the cell volume. This linear dependence shows that for the biggest rare earth atoms, the structure is less compact. In the lower frame (c) of Fig. 3 is represented the packing index vs the rare earth ionic radius.

Discussion

Interatomic bond distances and angles are collected in Table II. With these parameters we can calculate the geometrical features of all compounds and study the differences between them. The most important issue of this study should be the determination of the relevant geometrical changes in this structure when the size of the rare earth cation is varied.

In oxides where Ni^{2+} has a regular octa-

TABLE II

MAIN INTERATOMIC DISTANCES (Å) AND ANGLES (°) FOR R_2BaNiO_5 (R = Nd, Dy, Y, Ho, Er, Tm, Yb) OXIDES AT ROOM TEMPERATURE

	Nd_2BaNiO_5	Dy_2BaNiO_5	Y_2BaNiO_5	Ho_2BaNiO_5	Er_2BaNiO_5	Tm_2BaNiO_5	Yb_2BaNiO_5
Ni–O(1) (4×)	2.211(1)	2.189(2)	2.186(1)	2.185(1)	2.180(3)	2.174(2)	2.169(1)
–O(2) (2×)	1.9139(0)	1.8871(0)	1.8811(0)	1.8819(0)	1.8770(1)	1.8756(0)	1.8724(0)
R–O(1) (4×)	2.487(1)	2.427(2)	2.411(1)	2.417(1)	2.414(2)	2.401(1)	2.392(1)
–O(1) (2×)	2.3512(2)	2.253(2)	2.253(2)	2.249(2)	2.240(3)	2.222(2)	2.215(2)
–O(2) (1×)	2.364(1)	2.309(2)	2.292(1)	2.299(1)	2.292(2)	2.286(1)	2.277(1)
Ba–O(1) (8×)	2.973(1)	2.941(2)	2.939(1)	2.935(1)	2.924(2)	2.928(1)	2.925(1)
–O(2) (2×)	2.9660(0)	2.8900(0)	2.8814(0)	2.8805(0)	2.8715(1)	2.8607(0)	2.8533(0)
⟨O(1)–Ni–O(1)	80.89(9)	79.1(1)	78.63(9)	78.92(9)	79.1(1)	78.3(1)	78.04(9)
⟨O(1)–Ni–O(1)	99.11(9)	100.9(2)	101.37(9)	101.08(9)	100.8(2)	101.7(1)	101.96(9)

hedral coordination, Ni–O distances are about 2.08 Å (*16*). In the present case we have strongly distorted octahedra where the axial distance along a-axis is much shorter than the equatorial one. In addition the O(1)–Ni–O(1) angles in the basal plane are much different than the 90° of a regular octahedron. Figure 4 shows how these distances, together with the basal angle O(1)–Ni–O(1) vary when the different rare earth ions are present. The maximum variation of the axial Ni–O(2) distance (identical to the variation of the a-axis) over the average value is ±1.1%.

The relative variation of the Ni–O(1) distance is only ±0.9%. This small variation is accompanied by the change in the basal angle ⟨O(1)–Ni–O(1) of about ±1.8% with respect to the average value. The result is that the volume of the NiO_6 octahedron increases as does the ionic radius of the rare earth. Figure 5 shows this linear variation. The relative variation of the octahedra volume is ±3.5%. As expected, this value is slightly smaller than the variation of the cell volume.

It is interesting to point out that the ratio between the axial and equatorial distances is almost constant in this family of compounds ($\Delta = d$[Ni–O(2)]/d[Ni–O(1)] ≈ 0.86). So the main effect of the rare earth substitution is a slight increase of the NiO_6 volume and the change of the angle in the basal plane of the octahedra.

In summary we observe a highly distorted octahedron with two short axial distances and four long basal distances, which increases its volume conserving the axial/equatorial ratio, and varying the O(1)–Ni–O(1) angle in the basal plane. This is an unusual distortion, specially if we compare with the usual Cu behavior, where two long and four short distances are very commonly observed for the octahedral coordination. If we compare with similar Ni^{2+} in octahedral coordination, as is the case of La_2NiO_4, we also observe the two long and four short distances distortion (*29–34*).

Based on these structural data, and by means of semiempirical quantum chemistry calculations (*16*), the Y(Ni)-C6 oxide has been predicted to be a diamagnetic insulator by virtue of the expected low spin state of Ni^{2+}. These predictions are completely in disagreement with our experimental results (*21–25*).

The geometrical behavior of the NiO_6 octahedron in R_2BaNiO_5 presents a clear difference with the corresponding CuO_5 units in the R_2BaCuO_5 family of compounds (*17*), where the change of the rare earth does not affect the size of the Cu pyramids.

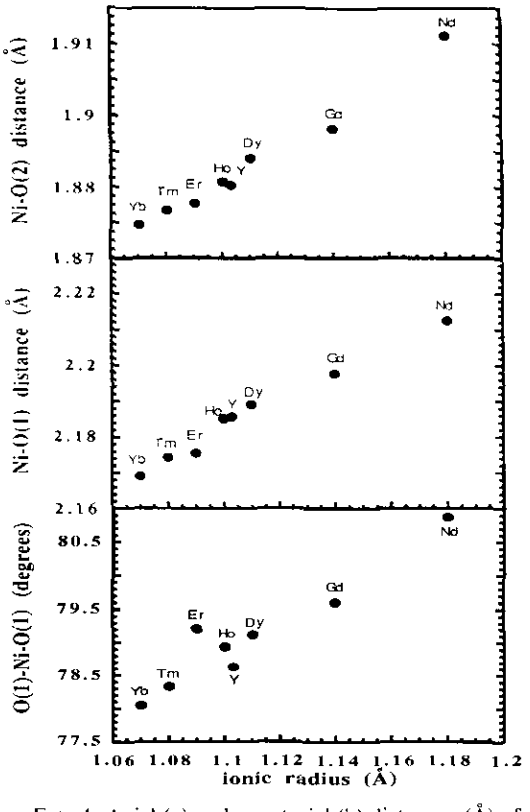

FIG. 4. Axial (a) and equatorial (b) distances (Å) of the NiO_6 octahedra, and the angle (c) O(1)–Ni–O(1) (°) vs rare earth ionic radius (Å).

Another important aspect is the behavior, as a function of the rare earth size, of the distances in the BaO_{10} coordination polyhedra. In this case there are two Ba–O distances, which also depend linearly on the ionic radius. The main variation (± 2.1%) is observed for the Ba–O(2) bond distance (see Table II). The RO_7 coordination polyhedra is characterized by three different distances. As expected, all the distances are linearly dependent with the ionic radius of the rare earth (see Table II).

All the above discussed geometrical changes suggest that the "chemical pressure effect" obtained by the change of the rare earth is mostly isotropic ("hydrostatic"). This manifests as an overall expansion of all the polyhedra in the structure and, consequently, a decrease of the packing index as rises the rare earth size.

The study of the valence of the different ions of the structure has been attempted by means of the Bond Valence Method. This method, described by Brown (*35*), gives a phenomenological relationship between the "formal" valence of a bond and the bond length. The relationship between the bond length (D) and bond valence (s) is given by $s_{ij} = \exp\{(R_o - D)/B\}$, where R_o is a constant characteristic of the particular cation–anion pair and $B = 0.37$ is a "universal" constant for all kinds of atoms. In perfect nonstrained structures, the bond valence sum (BVS) rule states that the formal charge (V_i) of the cation (anion) is equal to the sum of the bond valences around a cation (anion): $V_i = \sum_j s_{ij}$. This rule is satisfied only if the stress introduced by the coexistence of different structural units can be relieved by the existence of enough degrees of freedom in the crystallographic structure; i.e., the rule is violated in *highly* symmetric structures with several atoms in special positions. The departure from the BVS rule is a measure of the existing stress in the bonds of the structure. The present case of R_2BaNiO_5 oxides belongs to the type of structures where the BVS rule could be vio-

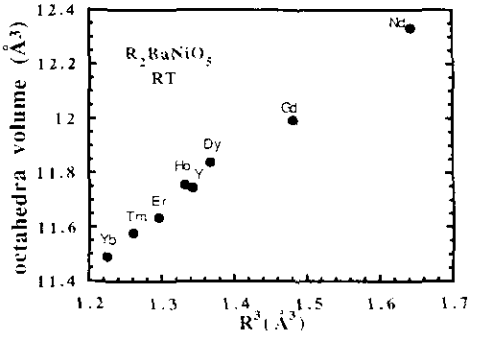

FIG. 5. Volume of the NiO_6 octahedra for the R_2BaNiO_5 family vs the cube of the rare earth ionic radius.

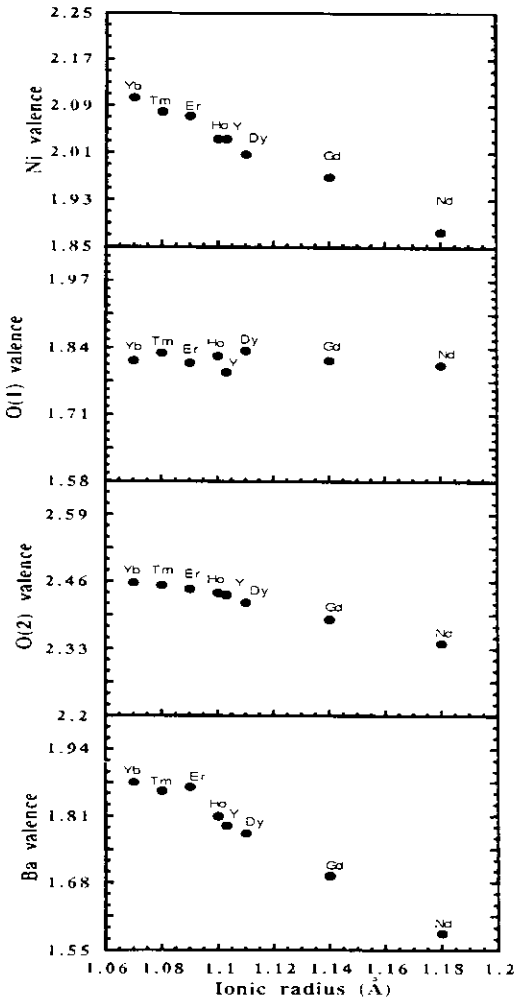

FIG. 6. BVS calculations for (a) Ni, (b) O(2), (c) O(1), and (d) Ba vs rare earth ionic radius (Å).

lated. All the calculations have been done from RT data where the R_0 parameters are known (*35, 36*), and diffraction data under similar conditions are available. We start assuming the formal valence states R^{3+}, Ni^{2+}, Ba^{2+}, and O^{2-}. Figure 6 shows the BVS for O(1) (V[O(1)]), for the different rare earth ions. V[O(1)] has an average value of 1.81 (±0.02) valence units (v.u.) without clear monotonic dependence on the ionic radius. This value is scarcely 10% smaller than expected. By contrast, V[O(2)] shows linear dependence on the rare earth size, varying between 2.35 and 2.45 v.u., i.e. 17–25% higher than the formal value 2 for O^{2-} (see Fig. 6). Due to the anomalous short Ni–O(2) distance, the O(1) is underbonded and the O(2) apex oxygen is strongly overbonded. Similar linear behavior is observed for Ba^{2+}, where a BVS between 1.9 and 1.6 is observed with a 5% to 20% difference with respect to the expected value. By contrast, V[Ni] is very close to 2, with a maximum deviation smaller than 4%. Nevertheless, inside this small variation there is a clear dependence on the ionic radius of the rare earth, which is also reflected by the volume change of the NiO_6 octahedra. A similar small variation (<4%) is observed for the BVS around the rare earth ions.

It is interesting to compare the case of the two dimorphic compounds (Tm and Yb) where a second structure is stable (*21*) with R(Ni)–C5. In the later structure, the maximum difference between the expected and calculated valences is obtained for Ni, in contrast to the present case. In summary, this phenomenological model indicates that the open shell ions (Ni^{2+} and R^{3+}) are better able to conserve their valences in the *Immm* structure. By contrast, the other ions, Ba^{2+} and O^{2-}, suffer a strong variation by the change of their corresponding bond distances. The most peculiar case is the O(2) which possess strong covalent bonding with Ni.

The root mean square of the BVS deviations for all the N atoms present in the asymmetric unit,

$$\mathrm{GII} = \sqrt{\frac{\sum_{i=1}^{N}\left\{\left(\sum_j s_{ij} - V_i\right)^2\right\}}{N}},$$

is a measure of the extent to which the BVS rule is violated over the whole structure (*37*). We call this value the *global instability index* (GII).

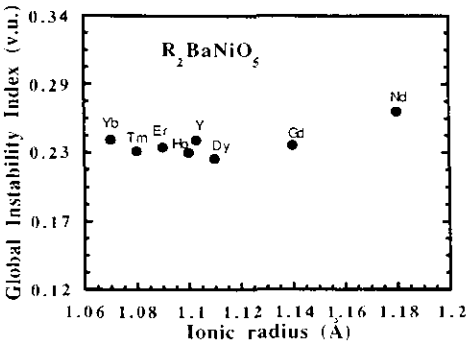

FIG. 7. Global instability index (GII), as defined in the text, of the different R_2BaNiO_5 compounds vs the rare earth ionic radius.

We have represented GII vs. ionic radii in Fig. 7. For the smallest rare earths there no obvious relationship between the instability index with the size of rare earth. On the other hand, the highest value of GII corresponds to Nd, which is at the same time the extreme of the series. In fact, no *R*(Ni)-C6 compounds could be prepared for *R* larger than Nd (i.e., Pr or La). Therefore, despite the lack of high-resolution data for the Gd–Sm compounds (very absorbing for neutrons), a regular increase in GII can be inferred for ionic radii going from 1.08 to 1.16 Å. Nevertheless, even if this variation is not much higher than the dispersion presented by the data, we could speculate that it is significant. In the *R*(Cu)–C5 family similar calculations give a critical value of GII around 0.16 v.u. (*17*). Further change of the ionic radius, for instance a size bigger than Sm^{3+}, should produce a highly distorted trigonal prism, which is unattainable; the new structure is stable with *R*(Cu)-C4P with space group *P4/mbm* (*17*). As suggested by Brown (*37*) and Armbruster *et al.* (*38*), GII values higher than 0.2 v.u. indicate the presence of intrinsic strains large enough to cause instability at room temperature. The large value (≈0.24 v.u.) of GII in the present case suggests that the *R*(Ni)–C6 compounds are under very high stress and may be metastable. It could be, as was already demonstrated for Tm and Yb (*21*), that these compounds were also dimorphic, being the *R*(Ni)–C5 the alternative structure which is able to relax the higher stress existing in *R*(Ni)–C6. As a matter of fact, the GII factor for Tm(Ni)–C5 and Yb(Ni)–C5 is much smaller (0.13 v.u.) in both cases. These values should be compared with the data presented in Fig. 7 of 0.23 v.u.

As was clearly demonstrated in the case of Tm_2BaNiO_5, if the synthesis temperature is low, the structure (Tm(Ni)-C6) is already partially formed, coexisting with the Tm (Ni)-C5 phase (*21*). Thermal treatments at intermediate temperatures produce pure Tm(Ni)-C5 structure. Further treatments at higher temperatures stabilized the Tm(Ni)-C6 phase. By the usual cooling procedures, the Tm(Ni)-C6 structure is maintained at RT. The back transformation of the Tm(Ni)-C6 to the Tm(Ni)-C5 structure seems to be difficult if the adequate temperature and reaction time are not properly selected. For that reason these compounds were only described as the *R*(Ni)-C6 structure by the Müller-Buschbaum group (*1–12*), because their synthesis by laser techniques produces very high temperatures. The chemical and thermal conditions to stabilize these two polymorphic phases may be difficult to obtain for the other rare earths. In summary, the *R*(Ni)-C6 structure seems to be stable at high temperatures. If a proper method is used this phase can be made metastable at RT. If not, the *R*(Ni)-C5 phase is more stable at RT. This is the case for the Yb(Ni)-C6 structure, where the use of BaO_2 as starting material seems to be important to stabilize at lower temperatures (around 920°C) the C6 phase which, otherwise, is the stable phase only at higher temperatures.

A schematic phase diagram of the polymorphism in *R*(Ni)-C6 is presented in Fig. 8. The shaded region represents hypothetical "soft chemistry" synthesis conditions, where the thermodynamically stable high

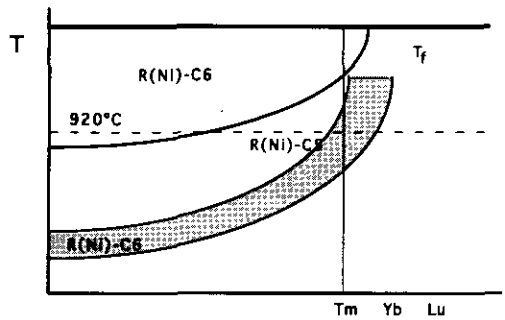

FIG. 8. Schematic phase diagram of the R_2BaNiO_5 compounds (see text for explanation). T_f means melting temperature.

temperature phase *R*(Ni)-C6 could be stabilized. In this region the *R*(Ni)-C5 structure could coexist. The continuous line represents the boundary at which the free energy of the C6 and C5 phases is equal. Under normal synthesis conditions the *R*(Ni)-C6 structure is obtained for *R* of atomic number below Tm. In these cases the transformation to the *R*(Ni)-C5 structure seems to be inhibited because the thermal energy is too low to overcome the energy barrier between the two phases. The upper solid line indicates the melting temperature boundary.

The analysis of the possible mechanisms of the C5 → C6 first order reconstructive polymorphic transformation is now in progress and a full account of this subject will be published in due time.

Acknowledgment

The authors thank the Institut Laue Langevin for making available the neutron beam time.

References

1. ST. SCHIFFLER AND HK. MÜLLER-BUSCHBAUM, *Z. Anorg. Allg. Chem.* **540/541,** 243 (1986), **523,** 63 (1985), **532,** 10 (1986).
2. H. MEVS AND HK. MÜLLER-BUSCHBAUM, *J. Less-Common Met.* **152,** 139 (1989).
3. ST. SCHIFFLER AND HK. MÜLLER-BUSCHBAUM. *J. Less-Common Met.* **128,** 117 (1987).
4. ST. SCHIFFLER AND HK. MÜLLER-BUSCHBAUM, *Monatsh. Chem.* **117,** 465 (1986); **118,** 741 (1987).
5. H. MEVS AND HK. MÜLLER-BUSCHBAUM, *Z. Anorg. Allg. Chem.* **573,** 128 (1989), **574,** 172 (1989).
6. HK. MÜLLER-BUSCHBAUM AND D. SCHLÜTER, *J. Less-Common Met.* **166,** L7 (1990).
7. HK. MÜLLER-BUSCHBAUM AND P. SONNE, *J. Less-Common Met.* **167,** 185 (1990); **167,** 193 (1990).
8. HK. MÜLLER-BUSCHBAUM AND S. MÖHR, *J. Less-Common Met.* **170,** 127 (1991).
9. HK. MÜLLER-BUSCHBAUM AND I. RÜTER, *Z. Anorg. Allg. Chem.* **572,** 181 (1989).
10. HK. MÜLLER-BUSCHBAUM AND E. KLÜVER, *Z. Anorg. Allg. Chem.* **612,** 14 (1992).
11. U. LEHMANN AND HK. MÜLLER-BUSCHBAUM, *Z. Naturforsch B* **35** 389 (1980).
12. B. GRANDE AND HK. MÜLLER-BUSCHBAUM, *Z. Anorg. Allg. Chem.* **433,** 152 (1977).
13. C. MICHEL AND B. RAVEAU, *J. Solid State Chem.* **43,** 73 (1982).
14. C. MICHEL, L. ER-RAKHO, AND B. RAVEAU, *J. Solid State Chem.* **42,** 173 (1982).
15. M. TAIBI, J. ARIBE, J. DARRIET, A. MOQINE, AND A. BOUKHARI, *J. Solid State Chem.* **86,** 233 (1990).
16. J. K. BURDETT AND J. F. MITCHELL, *J. Am. Chem. Soc.* **112,** 6571 (1990).
17. A. SALINAS-SANCHEZ, J. L. GARCIA-MUÑOZ, J. RODRIGUEZ-CARVAJAL, R. SAEZ-PUCHE, AND J. L. MARTINEZ, *J. Solid State Chem.* **100,** 201 (1992).
18. J. AMADOR, E. GUTIERREZ-PUEBLA, M. A. MONGE, I. RASINES, J. A. CAMPA, J. M. GOMEZ DE SALAZAR, AND C. RUIZ-VALERO, *Solid State Ionics* **32/33,** 123 (1989).
19. J. AMADOR, E. GUTIERREZ-PUEBLA, M. A. MONGE, I. RASINES, C. RUIZ-VALERO, F. FERNANDEZ, R. SAEZ-PUCHE, AND J. A. CAMPA, *Phys. Rev. B* **42,** 7918 (1990).
20. D. J. BUTTREY, J. D. SULLIVAN, AND A. L. RHEINGOLD, *J. Solid State Chem.* **88,** 291 (1990).
21. A. SALINAS-SANCHEZ, R. SAEZ-PUCHE, J. RODRIGUEZ-CARVAJAL, AND J. L. MARTINEZ, *Solid State Commun.* **78,** 481 (1991).
22. R. SAEZ-PUCHE, J. M. CORONADO, C. L. OTERO-DIAZ, AND J. M. MARTIN-LLORENTE, *J. Solid State Chem.* **93,** 461 (1991).
23. R. SAEZ-PUCHE, J. M. MARTIN-LLORENTE, AND J. M. CORONADO, *J. Less-Common Met.* **175,** 131 (1991).
24. G. G. CHEPURKO, Z. A. KAZEI, D. A. KUDRJAVTSEV, R. Z. LEVITIN, B. V. MILL, M. N. POPOVA, AND V. V. SNEGIREV, *Phys. Lett. A* **157,** 81 (1991).
25. J. A. ALONSO, J. AMADOR, J. L. MARTINEZ, I. RASINES, J. RODRIGUEZ-CARVAJAL, AND R. SAEZ-PUCHE, *Solid State Commun.* **76,** 467 (1990).

26. J. RODRIGUEZ-CARVAJAL, *in* "Abstracts of the Satellite Meeting on Powder Diffraction of the XV Congress of the International Union of Crystallography," p. 127, Toulouse, 1990.
27. J. A. ALONSO, J. AMADOR, I. RASINES, AND J. L. SOUBEYROUX, *Acta Crystallogr. Sect. C* **47,** 249 (1991).
28. Y. Q. JIA, *J. Solid State Chem.* **95,** 184 (1991).
29. J. RODRIGUEZ-CARVAJAL, M. T. FERNANDEZ-DIAZ, AND J. L. MARTINEZ, *J. Phys. Condensed Matter* **3,** 3215 (1991), and reference therein.
30. G. DEMAZEAU, M. POUCHARD, AND P. HAGENMULLER, *J. Solid State Chem.* **18,** 159 (1976).
31. A. RABENAU AND P. EICKERLIN, *Acta Crystallogr.* **11,** 304 (1958).
32. P. ODIER, M. LEBLANC, AND J. CHOISNET, *Mater. Res. Bull.* **21,** 787 (1986).
33. Y. TAKEDA, R. KAUNO, O. YAMAMOTO, M. SAKANO, Y. BANDO, AND H. AKINAGA, *Mater. Res. Bull.* **25,** 293 (1990).
34. HK. MÜLLER-BUSCHBAUM AND U. LEHMANN, *Z. Anorg. Allg. Chem.* **447,** 47 (1978).
35. I. D. BROWN AND D. ALTERMATT, *Acta Crystallogr. Sect. B* **41,** 244 (1985) **41,** 240 (1985).
36. N. E. BRESE AND M. O'KEEFFE, *Acta Crystalogr. Sect. B* **47,** 192 (1991).
37. I. D. BROWN, *Z. Kristalogr.* **199,** 255 (1992).
38. T. ARMBRUSTER, F. RÖTHLISBERGER, AND F. SEIFERT, *Am. Mineral.* **75,** 847 (1990).